Supporting Information

Quantum Plasmonic Immunoassay Sensing

Nuttawut Kongsuwan,[†,¶] Xiao Xiong,[‡,¶] Ping Bai,[‡] Jia-Bin You,[‡] Ching Eng Png,[‡]

Lin Wu,[*,‡] and Ortwin Hess[*,†]

†*The Blackett Laboratory, Prince Consort Road, Imperial College London, London SW7
2AZ, United Kingdom*

‡*Institute of High Performance Computing, A*STAR (Agency for Science, Technology and
Research), 1 Fusionopolis Way, #16-16 Connexis, Singapore 138632, Singapore*

¶*N.K.and X.X. contributed equally to this work.*

E-mail: wul@ihpc.a-star.edu.sg; o.hess@imperial.ac.uk

Section S1. Optical Lamb shift of an emitter label

The results in Fig. 2b show a shift between the emitter frequency at the maximum sensitivity enhancement $\omega_e = 2.03$ eV and the gap plasmonic resonance $\omega_p = 1.89$ eV. This shift is a result of the optical Lamb shift[1] where the emitter experiences back-scattered fields from its surroundings. We elaborate on this effect by placing a single emitter at different positions **1**, **2** and **3** (black, red and blue dots in Fig. S1a), with the coordinates $\mathbf{r_1} = (0, 0, 0)$ nm, $\mathbf{r_2} = (42, 0, 0)$ nm, and $\mathbf{r_3} = (21, 21, 0)$ nm. The emitter's polarization is set along the x-axis with transition frequency $\omega_e = 2.03$ eV. The electric field distribution of the bare hemisphere dimer is plotted in Fig. S1b. It shows that the electric field is the strongest at position **1** and the weakest at position **3**.

Figure S1c shows the spectra of the emitter at each position, which are the Fourier

transforms $\mathcal{F}[P] = \int P(t)exp(-i\omega t)\mathrm{d}t$ of the emitter's polarization density in Eq. 7-8. At positions **2** and **3** (red and blue curves), the coupling between the emitter and the plasmonic environment leads to the red-shifted emitter frequency (major peaks) compared to $\omega_\mathrm{e} = 2.03$ eV of the emitter in vacuum (gray curve). Stronger electric field results in a larger Lamb shift. Note that, the minor peaks at 1.89 eV represent for the plasmonic resonance. At position **1** where the electric field is the strongest, the emitter resonance experiences the largest red-shift and reaches values around the plasmonic resonance $\omega_\mathrm{p} = 1.89$ eV. Meanwhile, the emitter and plasmon-polaritons enter into the strong coupling regime, where the Rabi splitting results in two comparable peaks centered at 1.89 eV. In other words, the optical Lamb shift changes the emitter resonance from 2.03 eV to 1.89 eV, and results in the sensitivity enhancement peaked at 2.03 eV (Fig. 2b) when $\omega_\mathrm{p} = 1.89$ eV.
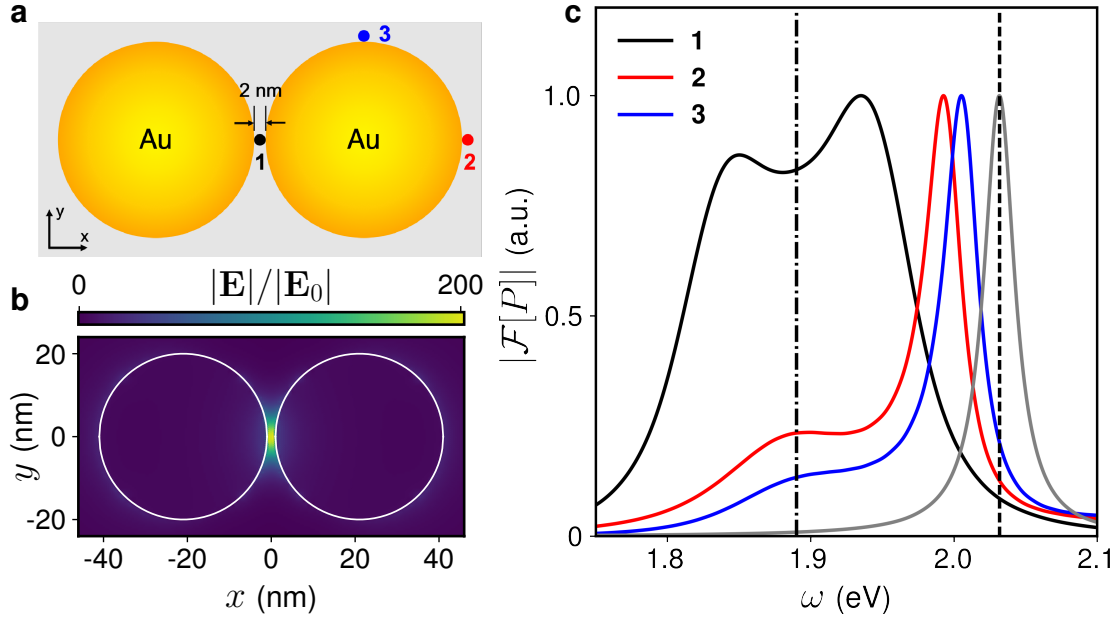

Figure S1: Optical Lamb shift of a single emitter due to the interaction with gap plasmons. (a) Top-view schematic diagram of the single emitter's position near the hemisphere dimer. The black, red and blue dots indicate the position of the emitter $\mathbf{r} = \mathbf{r_1}$, $\mathbf{r_2}$ and $\mathbf{r_3}$, respectively. (b) The xy-plane electric field distribution at $\omega = 1.89$ eV for an empty hemisphere dimer, where $|\mathbf{E}(\mathbf{r_1})|/|\mathbf{E_0}| = 194.8$, $|\mathbf{E}(\mathbf{r_2})|/|\mathbf{E_0}| = 11.9$ and $|\mathbf{E}(\mathbf{r_3})|/|\mathbf{E_0}| = 8.79$. (c) The Fourier transforms of the emitter's polarization densities $|\mathcal{F}[P]|$ at positions $\mathbf{r_1}$ (black), $\mathbf{r_2}$ (red) and $\mathbf{r_3}$ (blue). $|\mathcal{F}[P]|$ of an emitter in vacuum is also shown as a gray curve. The dashed line at $\omega = 2.03$ eV denotes the emitter's transition frequency ω_e, and the dash-dotted line at $\omega = 1.89$ eV denotes the gap plasmonic resonance ω_p.

Section S2. Location of the emitter label

For the hemisphere dimers with gap size $d > 2$ nm in Fig. 2c, the analyte-emitter complexes are not kept at the gap center $\mathbf{r} = \mathbf{0}$. Instead, they are placed 1 nm away from the gold hemisphere on the right, as summarized in Table S1. The reason for doing so is to ensure efficient coupling between the emitter label and plasmon-polaritons. In the following, we will prove this by placing the analyte-emitter complex at different locations.

We first define the distance between the emitter label and the hemisphere surface as l, as illustrated in the inset of Fig. S2a. Taking the case of $d = 6$ nm as an example, we calculate the extinction spectrum as the emitter label is moved with $l = 3, 2, 1$ nm, as shown in Fig. S2a. The Rabi splitting $\delta\omega$ is extracted and summarized in Fig. S2b, where the emitter gives a better performance at $l = 1$ nm.

For a dimer gap with $d = 3$–6 nm, the extinction spectra when the emitter is placed in the gap center and 1 nm away from the hemisphere are compared in Fig. S3. It shows that the sensitivity improvement offered by placing the emitter label at the optimized positions $\mathbf{r_e}$ is small in the case of small gaps, but becomes more significant at larger gap size.

Table S1: Position of the emitter label $\mathbf{r_e}$ for hemisphere dimer with gap $d = 2$–6 nm.

d (nm)	2	3	4	5	6
$\mathbf{r_e}$ (nm)	(0.0, 0, 0)	(0.5, 0, 0)	(1.0, 0, 0)	(1.5, 0, 0)	(2.0, 0, 0)

Section S3. Quasinormal modes

The mth-order gap plasmonic mode can be represented as a quasi-normal mode (QNM) with complex frequency $\tilde{\omega}_m = \omega_m - i\kappa_m$, where the real part ω_m describes its resonance frequency and the imaginary part κ_m describes the corresponding linewidth.[2] Given the electric field $\tilde{\mathbf{E}}_m(\mathbf{r_e})$ of mth-order QNM at position $\mathbf{r_e}$, the local mode volume and Purcell factor are then
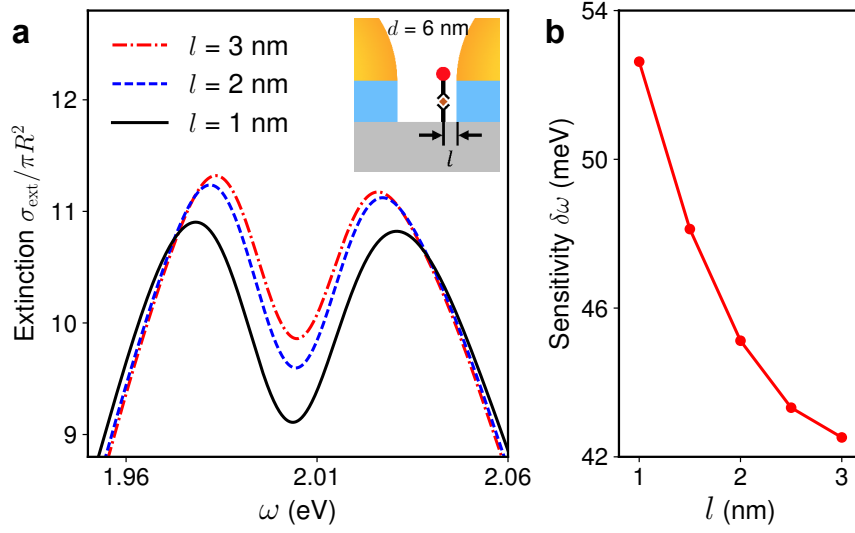
Figure S2: Extinction cross-sections and detection sensitivities of single-analyte detection at different locations for the hemisphere dimer with gap size 6 nm. (a) Extinction cross-section σ_{ext} for emitter labels located at $l = 3$ nm (red dash-dotted line), $l = 2$ nm (blue dashed line) and $l = 1$ nm (black solid line) away from the right gold hemisphere. (b) The splitting-type sensitivity $\delta\omega$ as a function of the distance l.
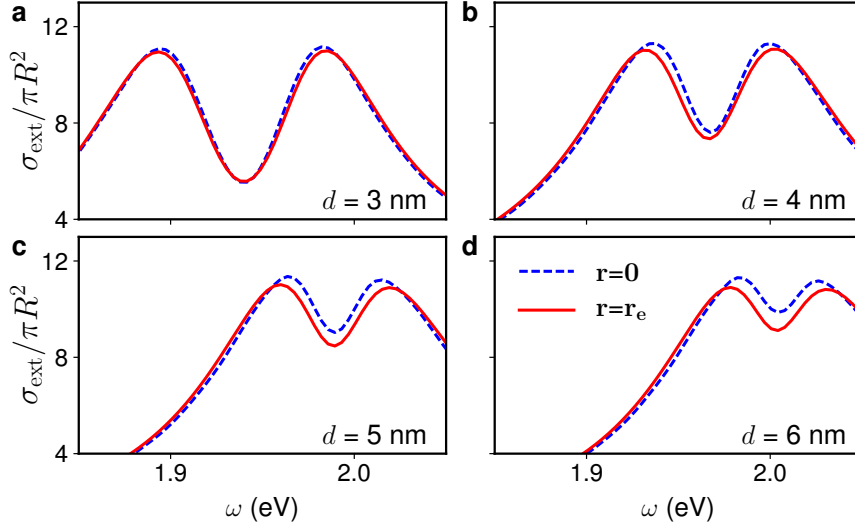

Figure S3: Extinction cross-sections of single-analyte detection at non-optimized and optimized locations. ((a)-(d)) Extinction cross-section σ_{ext} for emitter labels at location $\mathbf{r} = \mathbf{0}$ and $\mathbf{r} = \mathbf{r_e}$ for hemisphere dimer with gap size $d = 3$–6 nm.

4

evaluated as:[3]

$$V_m(\mathbf{r_e}) = \frac{1}{2\varepsilon_0\varepsilon_{\mathrm{B}}[\tilde{\mathbf{E}}_m(\mathbf{r_e}) \cdot \mathbf{n_e}]^2},\tag{S1}$$

$$F_m(\mathbf{r_e};\omega) = \frac{3}{4\pi^2}\mathrm{Im}\left[\left(\frac{\lambda_m}{n_{\mathrm{B}}}\right)^3 \frac{Q}{V_m(\mathbf{r_e})}\frac{\omega_m^2\kappa}{\omega\tilde{\omega}_m(\tilde{\omega}_m - \omega)}\right].\tag{S2}$$

In this study, we denote the the 1$^{\mathrm{st}}$-order gap plasmonic mode with complex frequency $\tilde{\omega}_1 = \omega_1 - i\kappa_1 = \omega_{\mathrm{p}} - i\kappa$. The Purcell factor $F_{m=1}(\mathbf{r_e};\omega_{\mathrm{p}})$ of the 1$^{\mathrm{st}}$-order gap plasmonic mode is then evaluated in the FDTD environment using the technique developed by Ge et $al.$[4,5]

Section S4. Multi-mode Purcell enhancement estimations

To predict the photoluminescence (PL) spectra in Fig. 3a, the interaction between a gap plasmonic mode and an emitter label is analyzed within the cavity quantum electrodynamics (cQED) framework. We assume that the 1$^{\mathrm{st}}$-order gap plasmonic mode can be well approximated as a single cavity mode with a bosonic operator a and frequency ω_{p}. The emitter label is treated as a two-level system with a Pauli-1/2 operator σ and frequency ω_{e}'. The Jaynes-Cummings Hamiltonian under the unitrary transformation with operator $U = \exp(-i\omega_{\mathrm{p}}a^\dagger at)$ is written as:

$$H = (\omega_{\mathrm{e}}' - \omega_{\mathrm{p}})\sigma^\dagger\sigma + g(a\sigma^\dagger + a^\dagger\sigma),\tag{S3}$$

where $g = \sqrt{F_{m=1}(\mathbf{r_e};\omega_{\mathrm{p}})\gamma_0\kappa/2}$ is the coupling strength,[6] and $F_{m=1}(\mathbf{r_e};\omega_{\mathrm{p}})$ is the local Purcell factor of the 1$^{\mathrm{st}}$-oder ($m = 1$) gap plasmon mode at the emitter's location $\mathbf{r_e}$.

The PL spectra can be calculated from the steady-state number of photons $\langle a^\dagger a\rangle$ in the system, subject to the decoherence from an external reservoir. The steady-state solution can be found by solving the Lindblad master equation $\partial\rho/\partial t = \mathcal{L}\rho = 0$. The Lindblad operator

is defined as:

$$\mathcal{L}\rho = -i[H, \rho] + \frac{\kappa}{2}(2a\rho a^\dagger - a^\dagger a\rho - \rho a^\dagger a)$$
$$+ \frac{\gamma}{2}(2\sigma\rho\sigma^\dagger - \sigma^\dagger\sigma\rho - \rho\sigma^\dagger\sigma) \qquad (S4)$$
$$+ \frac{\Lambda}{2}(2\sigma^\dagger\rho\sigma - \sigma\sigma^\dagger\rho - \rho\sigma\sigma^\dagger) + \frac{\Gamma}{2}(\sigma_z\rho\sigma_z - \rho),$$

where $\kappa = -\text{Im}[\tilde{\omega}_1]$ is the cavity decay rate, $\Gamma = 13$ meV is the dephasing rate, and $\Lambda = 1$ meV is the incoherent pumping rate, which is sufficiently weak so that $\langle a^\dagger a \rangle \ll 1$. The relaxation rate γ is defined as the total decay rate due to higher-order plasmonic modes, which behave as a single collective pseudomode:[7,8]

$$\gamma(\mathbf{r_e}; \omega) = F_{m>1}(\mathbf{r_e}; \omega)\gamma_0(\omega), \qquad (S5)$$

where $F_{m>1}(\mathbf{r_e}; \omega'_e)$ is the Purcell factor of the higher-order modes. We estimate $F_{m>1}$ by subtracting $F_{m=1}$ from the total Purcell factor F_{tot} which is defined as:

$$F_{\text{tot}}(\mathbf{r_e}; \omega) = \frac{\gamma(\mathbf{r_e}; \omega)}{\gamma_0(\omega)} = \frac{\text{Im}[\mathbf{n_e} \cdot \mathbf{G}(\mathbf{r_e}, \mathbf{r_e}; \omega) \cdot \mathbf{n_e}]}{\text{Im}[\mathbf{n_e} \cdot \mathbf{G_0}(\mathbf{r_e}, \mathbf{r_e}; \omega) \cdot \mathbf{n_e}]}, \qquad (S6)$$

where $\mathbf{G}$ and $\mathbf{G_0}$ are dyadic Green functions[1] of the hemisphere dimer and the homogeneous background with refractive index $n_\text{B} = 1.33$, respectively. By placing a dipole source with the same dipole moment μ, position $\mathbf{r_e}$, and orientation $\mathbf{n_e}$ as the quantum emitter, we can obtain $\mathbf{G}$ from the dipole source power:

$$\frac{\text{d}W}{\text{d}t} = \frac{\omega^3\mu^2}{2\varepsilon\varepsilon_0 c^2}\text{Im}[\mathbf{n_e} \cdot \mathbf{G}(\mathbf{r_e}, \mathbf{r_e}; \omega) \cdot \mathbf{n_e}]. \qquad (S7)$$

Figure S4 shows $F_{m=1}$, $F_{m>1}$ and F_{tot} for the hemisphere dimer with gap size $d = 2$–6 nm, where the dipole source and emitter are placed at position $\mathbf{r_e}$.

Finally, the PL spectra are calculated from the Wiener-Khintchine theorem and the

quantum regression theorem:[9]

$$\sigma_{\mathrm{PL}}(\omega) \propto -\mathrm{Re}\{\mathrm{Tr}[a^{\dagger}(\mathcal{L} - i(\omega - \omega_{\mathrm{p}})\mathcal{I})^{-1}a\rho_0]\}, \tag{S8}$$

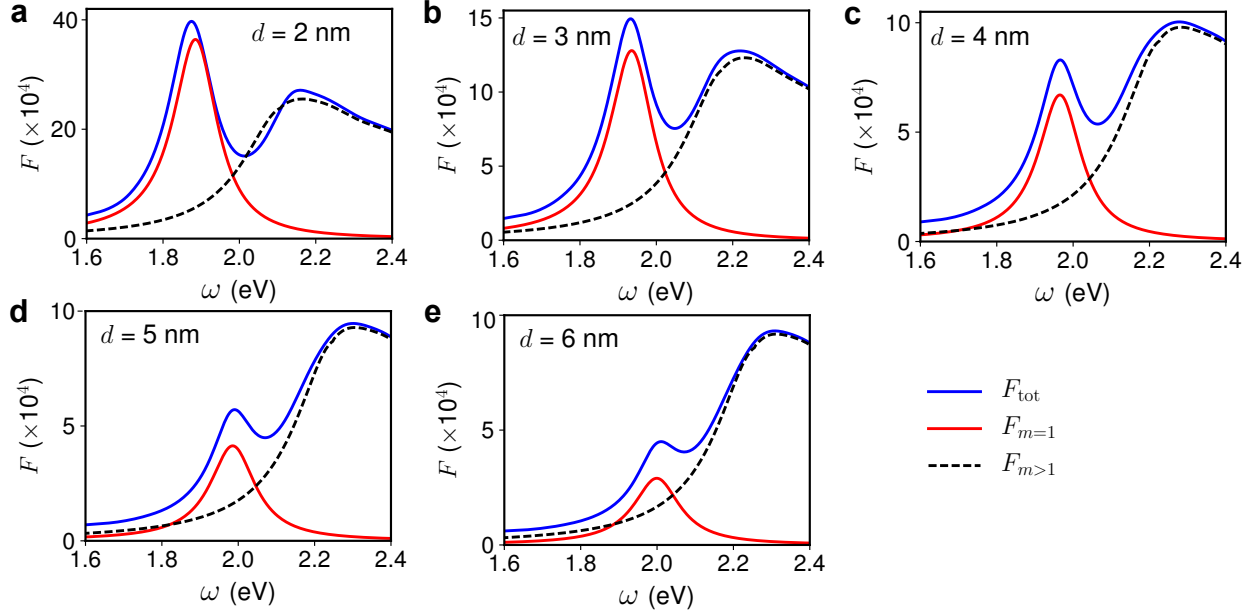where ρ_0 is the steady-state solution to Eq. S4.

Figure S4: Multi-mode Purcell factors of the hemisphere dimer. (a)-(e) The total Purcell factor F_{tot} calculated by using a dipole source (blue lines), the Purcell factor of the 1$^{\mathrm{st}}$-order QNM $F_{m=1}$ (red lines) and higher-order QNMs $F_{m>1}$ (black dashed lines) for an emitter placed at position $\mathbf{r_e}$ in the dimer with gap size $d = 2$–6 nm.

Section S5. Statistical study of multi-analyte detection

Figure 4 demonstrates the classical and quantum regimes for detection of randomly distributed multiple analyte-emitter complexes using the hemisphere dimer with gap size $d = 2$ nm. We obtained the random analyte-emitter complexes by assigning them on a 2D hexagonal lattice with the center-to-center distance between adjacent hexagons being $a = 2$ nm, which ensures non-overlapping distribution of the analyte-emitter complexes and corresponds to a surface density of lattice sites $(2/\sqrt{3})a^{-2} = 0.289$ nm^{-2}. A random number generator

was used to determine whether a given lattice site is occupied by an analyte-emitter complex subject to occurrence probabilities of 0.1, 0.2, 0.3, 0.4, 0.5 and 0.6, which correspond to the average surface densities of emitters $S = 0.029, 0.058, 0.087, 0.115, 0.144$, and 0.173 nm^{-2}, respectively. In order to find the average numbers of analyte-emitter complexes surrounding the plasmonic nanocavity, we define the cavity mode area as the region where the electric field intensity $|\mathbf{E}|^2$ exceeds 10% of its maximum as $|\mathbf{E}(x, y, 0)|^2 > 0.1|\mathbf{E}(x, y, 0)|^2_{\text{max}}$. This definition gives a cavity mode area of 35.75 nm^2 when $d = 2$ nm (Fig. 1c), which contains 10.3 lattice sites for analyte-emitter complexes. In this case, the average surface density of emitters and the number of emitters at each occurrence probability are summarized in Table S2. Note that, the number of emitters that practically participate in the coupling with plasmon-polaritons varies for each simulation sample. The number of emitters summarized here is only an average value.

In this study, 30 simulation samples for each surface density were taken, with the corresponding spectra of extinction cross-section σ_{ext} shown in Figs. S5-S10. With sparsely distributed analyte-emitter complexes, the extinction spectra are clean, exhibiting either incrementally shifted resonance (classical regime) or two split peaks (quantum regime). As the surface density of analyte-emitter complexes increases, the extinction spectra become irregular and show multiple peaks such that the line-shapes are no longer well-defined.

From these extinction spectra, we calculated their figure of merit (FoM) with Eq. 6, and plotted the frequency histogram of FoMs in Fig. S11. At low surface density, two sensing regimes are clearly observed, where the samples have either FoM < 0.3 or FoM > 0.3 depending on whether an analyte-emitter complex is located near the plasmonic hotspot. However, the boundary between the two regimes gradually vanishes at higher surface density, as the analytes tend to occupy all the vacancies on the substrate.
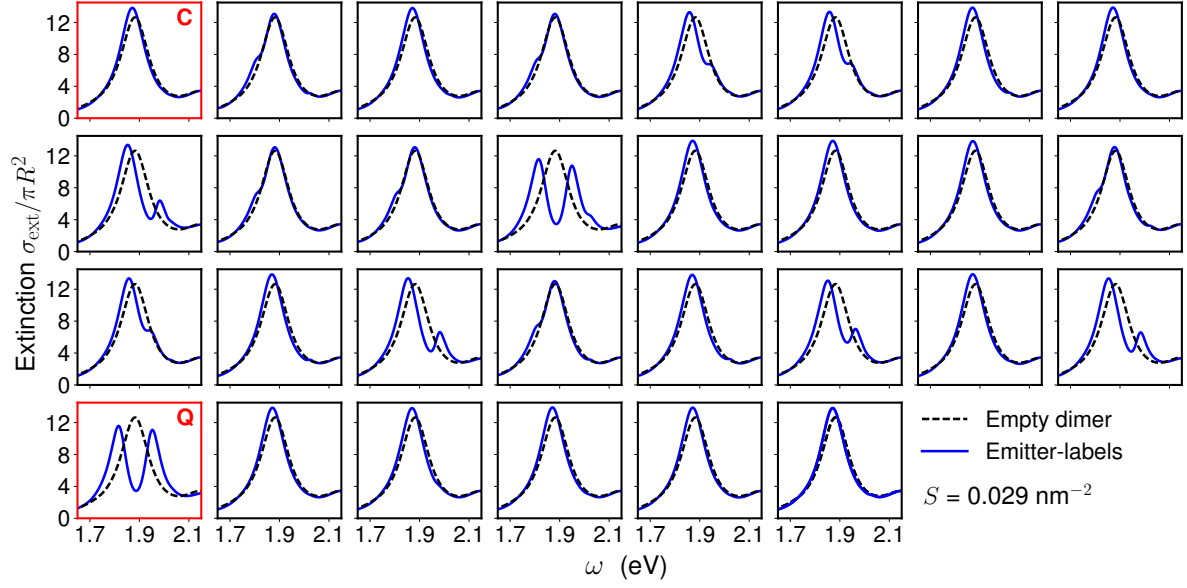
Figure S5: Random samples of extinction spectra. 30 random samples of extinction cross-sections σ_{ext} with analyte-emitter complex surface density $S = 0.029$ nm^{-2}. The C and Q highlighted in red denote the representatives in Fig. 4b for classical and quantum regimes, respectively.
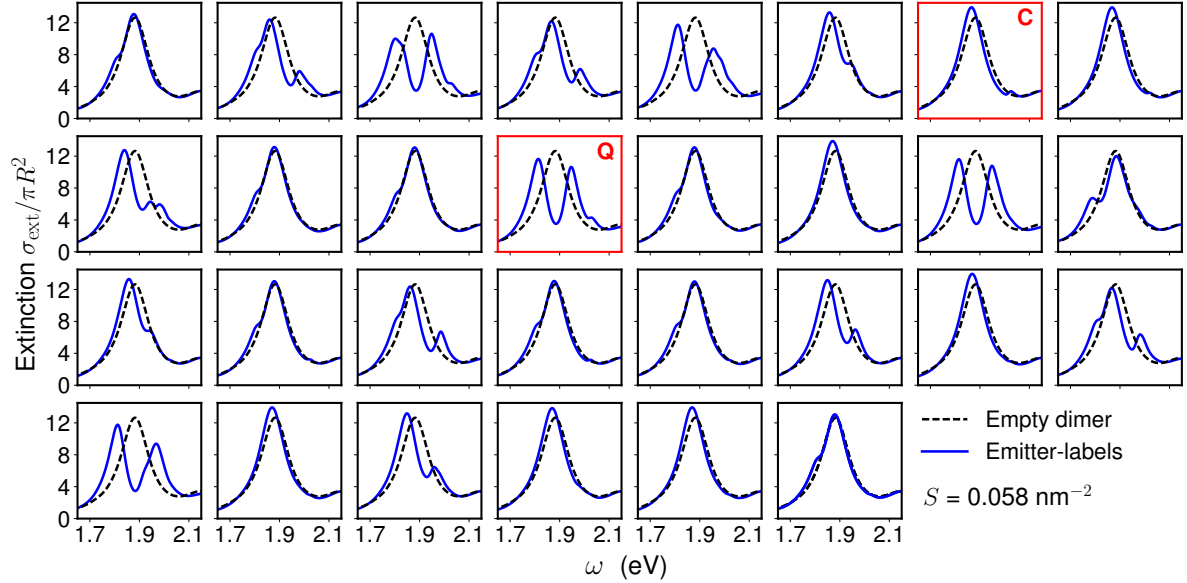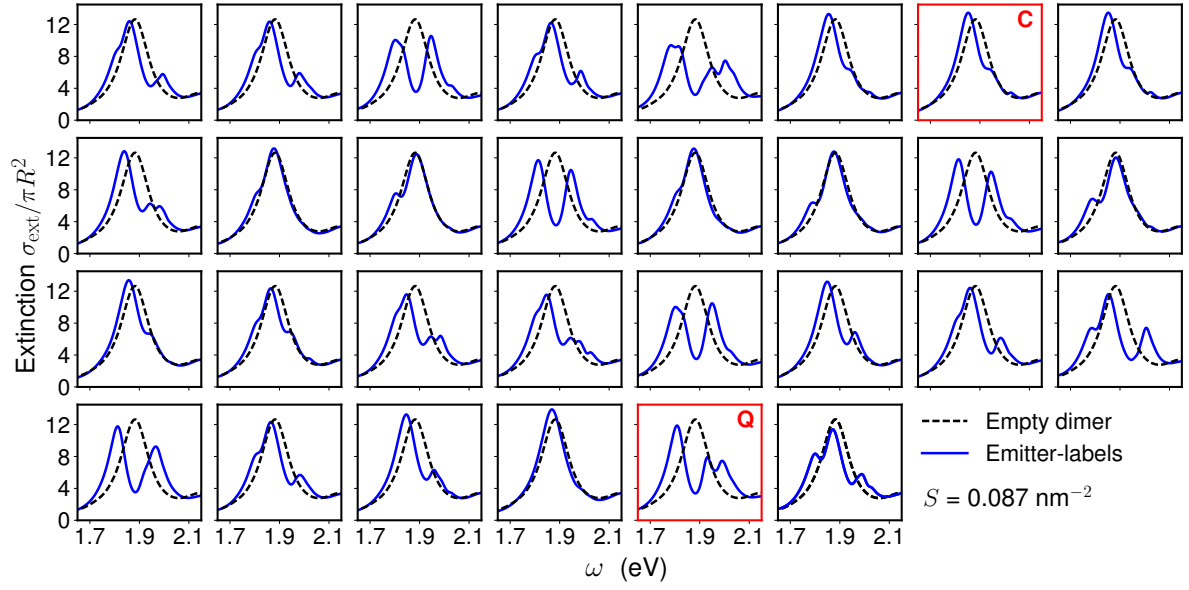

Figure S6: Random samples of extinction spectra. 30 random samples of extinction cross-sections σ_{ext} with analyte-emitter complex surface density $S = 0.058$ nm^{-2}. The C and Q highlighted in red denote the representatives in Fig. 4b for classical and quantum regimes, respectively.

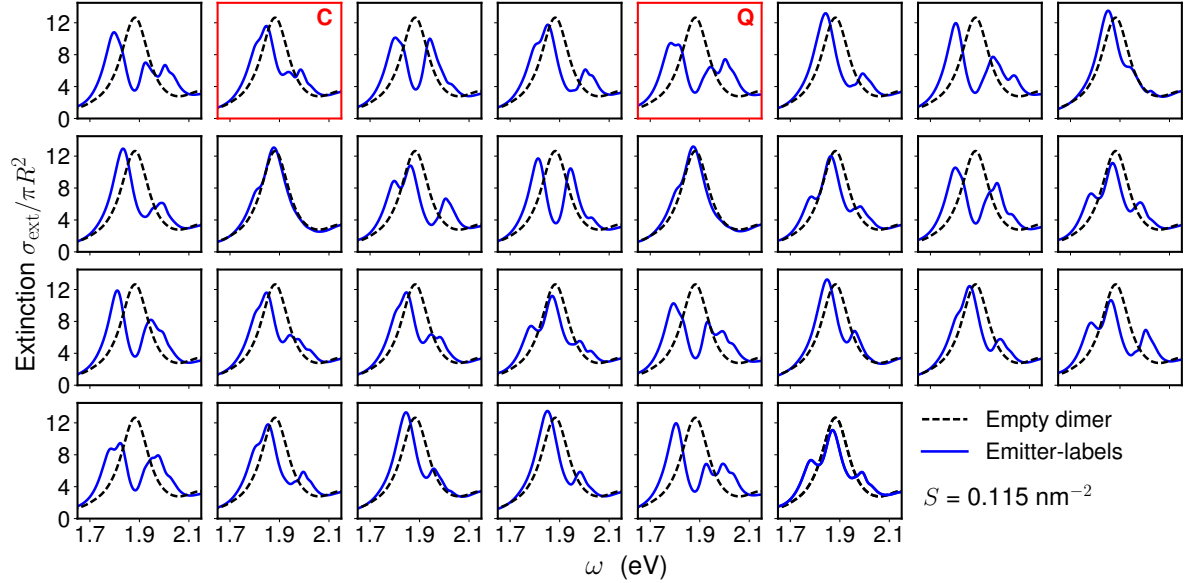Figure S7: Random samples of extinction spectra. 30 random samples of extinction cross-sections σ_{ext} with analyte-emitter complex surface density $S = 0.087$ nm^{-2}. The C and Q highlighted in red denote the representatives in Fig. 4b for classical and quantum regimes, respectively.

Figure S8: Random samples of extinction spectra. 30 random samples of extinction cross-sections σ_{ext} with analyte-emitter complex surface density $S = 0.115$ nm^{-2}. The C and Q highlighted in red denote the representatives in Fig. 4b for classical and quantum regimes, respectively.

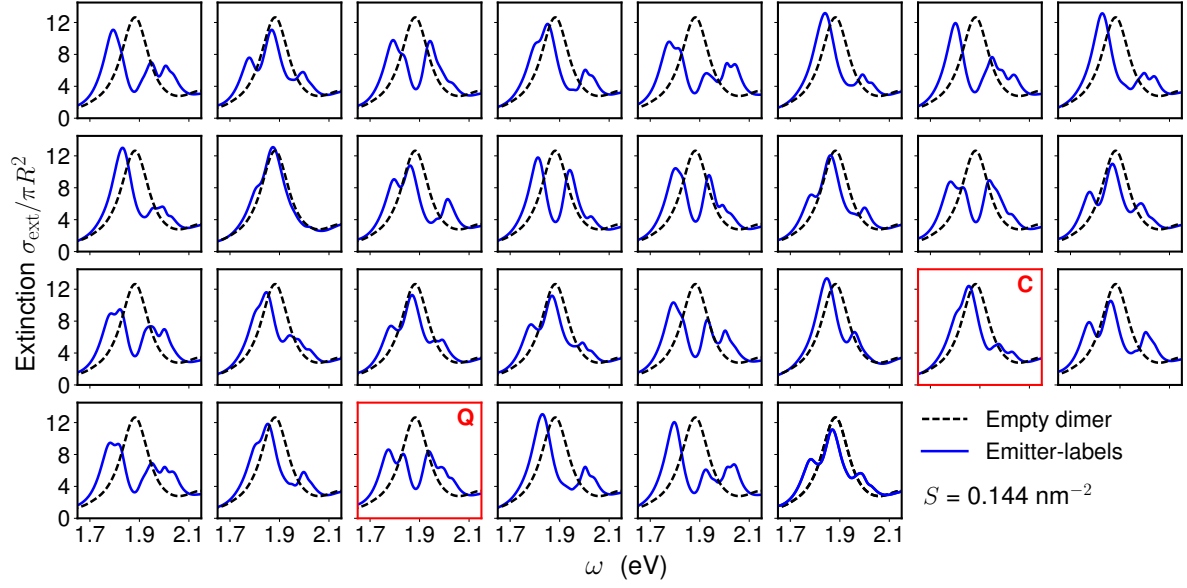Figure S9: Random samples of extinction spectra. 30 random samples of extinction cross-sections σ_{ext} with analyte-emitter complex surface density $S = 0.144$ nm^{-2}. The C and Q highlighted in red denote the representatives in Fig. 4b for classical and quantum regimes, respectively.
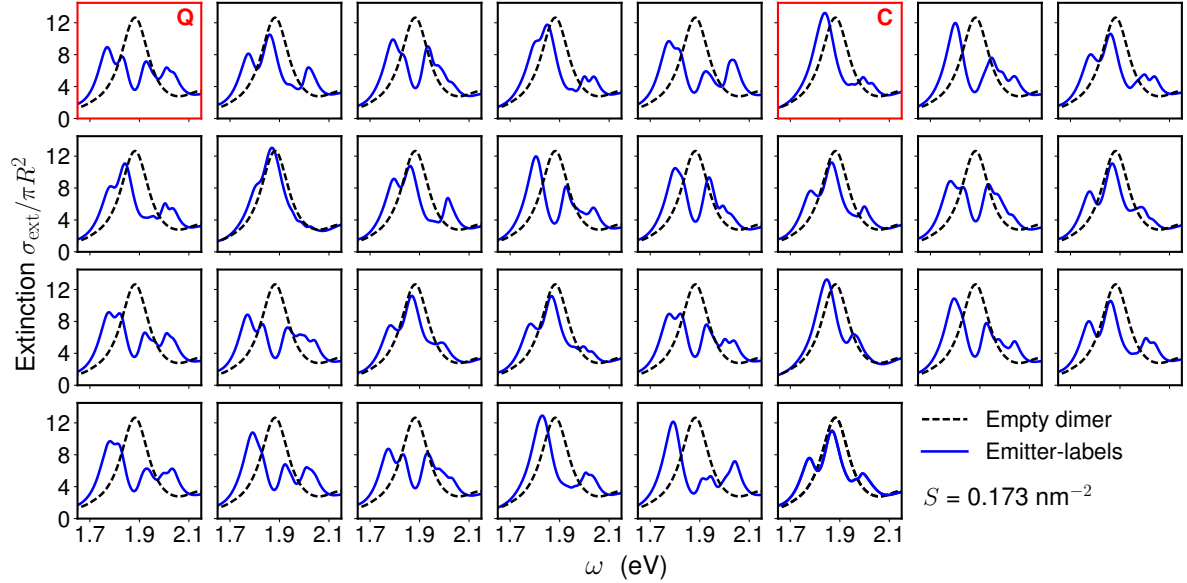

Figure S10: Random samples of extinction spectra. 30 random samples of extinction cross-sections σ_{ext} with analyte-emitter complex surface density $S = 0.173$ nm^{-2}. The C and Q highlighted in red denote the representatives in Fig. 4b for classical and quantum regimes, respectively.

Table S2: Average surface densities and average numbers of analyte-emitter complexes. The analyte-emitter complexes are randomly distributed with occurrence probabilities from 0.1 to 0.6 on a 2D hexagonal lattice with lattice constant $a = 2$ nm. The average emitter numbers are determined from the numbers of lattice sites within the area where $|\mathbf{E}(x, y, 0)|^2 > 0.1|\mathbf{E}(x, y, 0)|^2_{\max}$.

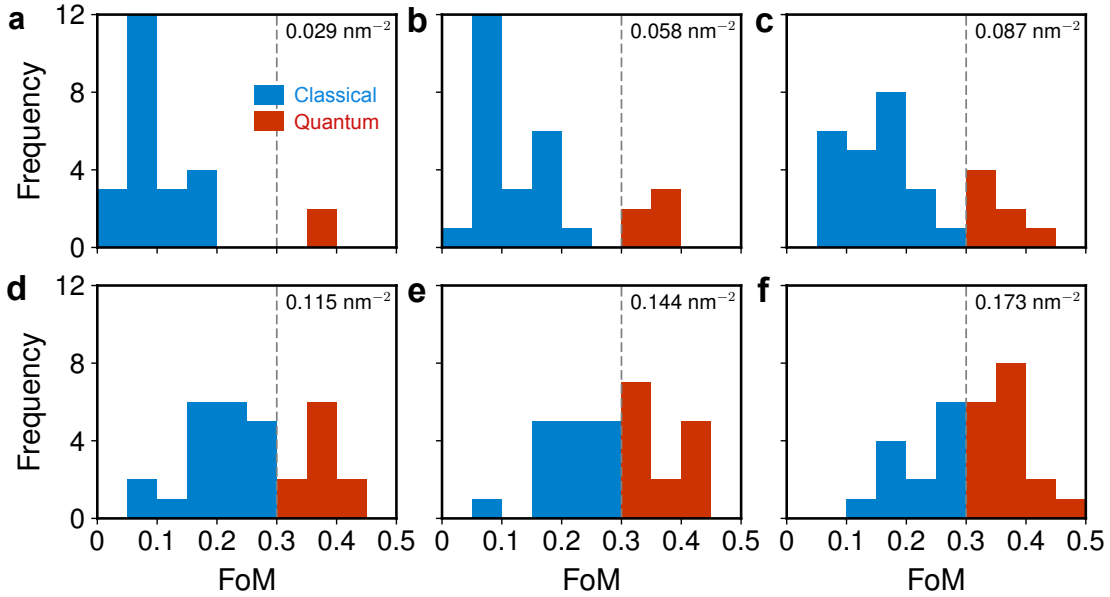| Occurrence probability	Average surface density (nm^{-2})	Average emitter number
0.1	0.029	1.03
0.2	0.058	2.06
0.3	0.087	3.10
0.4	0.115	4.13
0.5	0.144	5.16
0.6	0.173	6.19

Figure S11: Statistics on figure of merit with different surface density of analyte-emitter complexes. Histogram of FoM in Fig. 4c with surface density $S = 0.029, 0.058, 0.087, 0.115, 0.144$ and 0.173 nm^{-2}. The histogram is classified into two colors for classical regime (blue, FoM < 0.3) and quantum regime (red, FoM > 0.3), with dashed lines denoting the boundary.

References

(1) Novotny, L.; Hecht, B. *Principles of nano-optics*; Cambridge university press, 2012.

(2) Lalanne, P.; Yan, W.; Vynck, K.; Sauvan, C.; Hugonin, J.-P. *Laser Photonics Rev.* **2018**, *12*, 1700113.

(3) Sauvan, C.; Hugonin, J. P.; Maksymov, I. S.; Lalanne, P. *Phys. Rev. Lett.* **2013**, *110*, 237401.

(4) Ge, R. C.; Hughes, S. *Opt. Lett.* **2014**, *39*, 4235–4238.

(5) Ge, R. C.; Kristensen, P. T.; Young, J. F.; Hughes, S. *New J. P.* **2014**, *16*, 113048.

(6) Marquier, F.; Sauvan, C.; Greffet, J.-J. *ACS Photonics* **2017**, *4*, 2091–2101.

(7) Delga, A.; Feist, J.; Bravo-Abad, J.; Garcia-Vidal, F. J. *Phys. Rev. Lett.* **2014**, *112*, 253601.

(8) Chikkaraddy, R.; Turek, V. A.; Kongsuwan, N.; Benz, F.; Carnegie, C.; van de Goor, T.; de Nijs, B.; Demetriadou, A.; Hess, O.; Keyser, U. F.; Baumberg, J. J. *Nano Lett.* **2018**, *18*, 405–411.

(9) del Valle, E.; Laussy, F. P.; Tejedor, C. *Phys. Rev. B* **2009**, *79*, 235326.